This document was prepared in conjunction with work accomplished under Contract No. DE-AC09-96SR18500 with the U. S. Department of Energy.

DISCLAIMER

WSRC-TR-2005-00288

Computational Fluid Dynamics Model for Saltstone Vault 4 Vapor Space

Si Young Lee

June 17, 2005

Westinghouse Savannah River Company
Savannah River National Laboratory
Aiken, SC 29808

Prepared for the U.S. Department of Energy

Under Contract No. DE-AC09-96SR18500

SRNL
SAVANNAH RIVER NATIONAL LABORATORY

DISCLAIMER

Printed in the United States of America

Prepared For

U.S. Department of Energy

WSRC-TR-2005-00288

Keywords: Computational Fluid Dynamics, Saltstone Vault, Flow Patterns, Natural Convection, Heat Transfer

Computational Fluid Dynamics Model for Saltstone Vault 4 Vapor Space

Si Young Lee

June 2005

Westinghouse Savannah River Company
Savannah River National Laboratory
Aiken, SC 29808

Prepared for the U.S. Department of Energy

Under Contract No. DE-AC09-96SR18500

SRNL
SAVANNAH RIVER NATIONAL LABORATORY

(This Page Intentionally Left Blank)

Review and Approvals

S. Y. Lee, Author — Date 6/27/05
Eng. Modeling and Simulations Group, SRNL

G. A. Taylor, Technical Reviewer — Date 6/27/05
Waste Processing Tech. Section, SRNL

A. V. Staub, Customer Reviewer — Date 6/27/05
DWPF Process Eng.

C. P. Holding-Smith, Manager — Date 6/27/05
Eng. Modeling and Simulations Group, SRNL

J. E. Occhipinti, Manager — Date 6/27/05
DWPF Process Engineering

(This Page Intentionally Left Blank)

Table of Contents

Abstract 1

1. Introduction 1

2. Modeling Approach and Analysis Method 3

3. Results and Discussions 6

3.1 Benchmarking Results 7

Case 1: Turbulent isothermal flow in a pipe. 7

Case 2: Two-dimensional natural convection inside a rectangular enclosure with specified boundary temperatures 8

3.2 Results for the Saltstone Vault Model 12

4. Conclusions 32

5. References 33

List of Figures

Figure 1. Modeling domain of vapor space for Saltstone Vault 4 used for the present work. 2

Figure 2. Three-dimensional computational domain and meshes of the vapor space of Saltstone Vault 4 as used for the present modeling calculations. 4

Figure 3. Isothermal flow in a circular pipe..... 7

Figure 4. Natural convection test section inside a slit enclosure..... 9

Figure 5. Comparison of FLUENT6 predictions with theoretical predictions for Case A11

Figure 6. Comparison of FLUENT6 predictions with theoretical predictions for Case B11

Figure 7. Temperature contours near the lower end breathing hole at t = 7 hours..... 14

Figure 8. Temperature contours near the higher end breathing hole at t = 7 hours..... 15

Figure 9. Flow patterns near the lower end breathing hole at t = 7 hours..... 16

Figure 10. Flow patterns near the higher end breathing hole at t = 7 hours 17

Figure 11. Density distributions along the diagonal plane crossing the two ventilation holes..... 18

Figure 12. Density distributions near the lower end breathing hole at t = 7 hours showing the ambient heavier air is drawing into the vapor space of the Saltstone vault18

Figure 13. Temperature distributions at the mid-plane of the gas space showing the honeycomb-type heat transfer..... 19

Figure 14. Density distributions at the mid-plane of the gas space showing the honeycomb-type heat transfer..... 19

Figure 15. Velocity flow patterns at the mid-plane of the vapor space inside the vault.. 20

Figure 16. Gas upward velocity profile along the vertical lines A-A' and B-B' of the two ventilation holes indicating that the lower end hole has downward airflow patterns 21

Figure 17. Temperature distributions near the ventilation hole at the higher end of the vault during the 90 second transient period of the negative temperature gradient 22

Figure 18. Temperature distributions near the ventilation hole at the lower end of the vault during the 90 second transient period of the negative temperature gradient 22

Figure 19. Flow patterns near the ventilation hole at the higher end of the vault during the 90 second transient period of the negative temperature gradient 23

Figure 20. Flow patterns near the ventilation hole at the lower end of the vault during the 90 second transient period of the negative temperature gradient 24

Figure 21. Gas upward velocity profile along the vertical lines A-A' and B-B' of the two ventilation holes under the negative temperature gradient between the inner roof and top grout surface during early transient period (90 seconds of

transient time), indicating that both of the lower and higher holes have upward airflow patterns 25

Figure 22. Flow patterns near the ventilation hole at the higher end of the vault during the 180 second transient period of the negative temperature gradient 26

Figure 23. Flow patterns near the ventilation hole at the lower end of the vault during the 180 second transient period of the negative temperature gradient 27

Figure 24. Gas upward velocity profile along the vertical lines A-A' and B-B' of the two ventilation holes under the negative temperature gradient between the inner roof and top grout surface at 3-minute transient time, noting that the lower end hole has the gas flow patterns switched from the upward flow of the 90-second transient to the downward one of the later transient 28

Figure 25. Temperature contours near the ventilation hole at the lower end of the vault during the 180 second transient period of the negative temperature gradient showing that the hot gas is leaving the vapor space through the ventilation hole 29

Figure 26. Temperature contours near the ventilation hole at the lower end of the vault during the 180 second transient period of the negative temperature gradient showing that the vapor space region near the ventilation hole of the lower end has ambient temperature 30

Figure 27. Qualitative gas circulation patterns obtained by the present CFD modeling calculations for the vapor space of Saltstone vault #4, showing that the ambient air comes into the vapor space of the vault through the ventilation hole located near the lower end 31

List of Tables

Table 1. Reference modeling conditions used for the baseline calculations in the present modeling analysis. 5

Table 2. Modeling conditions for negative temperature gradient between the inner roof and top grout surface 6

Table 3. Comparison of FLUENT 6 prediction with theoretical value. 8

Table 4. Comparison of maximum velocities predicted by FLUENT 6 and theoretical values. 10

Table 5. Quantitative results for the air flowrate coming into the vapor space through the ventilation hole near the lower end of the vault under the two modeling conditions considered in the present work 32

Abstract

Computational fluid dynamics (CFD) methods have been used to estimate the flow patterns for vapor space inside the Saltstone Vault #4 under different operating scenarios. The purpose of this work is to examine the gas motions inside the vapor space under the current vault configurations.

A CFD model took three-dimensional transient momentum-energy coupled approach for the vapor space domain of the vault. The modeling calculations were based on prototypic vault geometry and expected normal operating conditions as defined by Waste Solidification Engineering. The modeling analysis was focused on the air flow patterns near the ventilated corner zones of the vapor space inside the Saltstone vault.

The turbulence behavior and natural convection mechanism used in the present model were benchmarked against the literature information and theoretical results. The verified model was applied to the Saltstone vault geometry for the transient assessment of the air flow patterns inside the vapor space of the vault region using the boundary conditions as provided by the customer.

The present model considered two cases for the estimations of the flow patterns within the vapor space. One is the reference baseline case. The other is for the negative temperature gradient between the roof inner and top grout surface temperatures intended for the potential bounding condition. The flow patterns of the vapor space calculated by the CFD model demonstrate that the ambient air comes into the vapor space of the vault through the lower-end ventilation hole, and it gets heated up by the Benard-cell type circulation before leaving the vault via the higher-end ventilation hole. The calculated results are consistent with the literature information.

1. Introduction

Waste Solidification (WS) Engineering has been evaluating the potential flammable conditions in the vapor space of Saltstone Vault #4 in response to a declared possible inadequacy to the Safety Analysis. In order to help assess the potential for benzene layer formation on top of the grout, Savannah River national Laboratory (SRNL) was requested to develop a computational model of the Vault # 4 vapor space to estimate the nature of vapor movement inside the vault. The vault geometrical configurations are shown in Fig. 1.

The vault has two breathing holes, which are located along the diagonally opposed location as shown in Fig. 1. The main objective of this work is to examine the gas motions inside the vapor space under the current vault configurations by taking a computational fluid dynamics (CFD) modeling approach [1]. The modeling domain of the present analysis is shown in Fig. 1. The modeling analysis was focused on the impacts of two breathing holes on the gas flow patterns due to the mass and energy exchanges between the cooler gas of the ambient air and the warmer vapor space gas of the vault, especially, under hot summer conditions.

In the present work two modeling cases were considered. One case represents the nominal reference conditions for the baseline analysis. The other is for the case with

negative temperature gradient, that is, Saltstone vault has the inner roof surface temperature higher than the top grout surface. The latter case corresponds to the potential bounding case in terms of flammable gas mixing, which is expected under the hot summer conditions. The modeling results will assist in understanding the qualitative gas flow patterns within the vapor space of the Saltstone vault and ambient air circulation paths through the two ventilation holes under the potential operating scenarios.

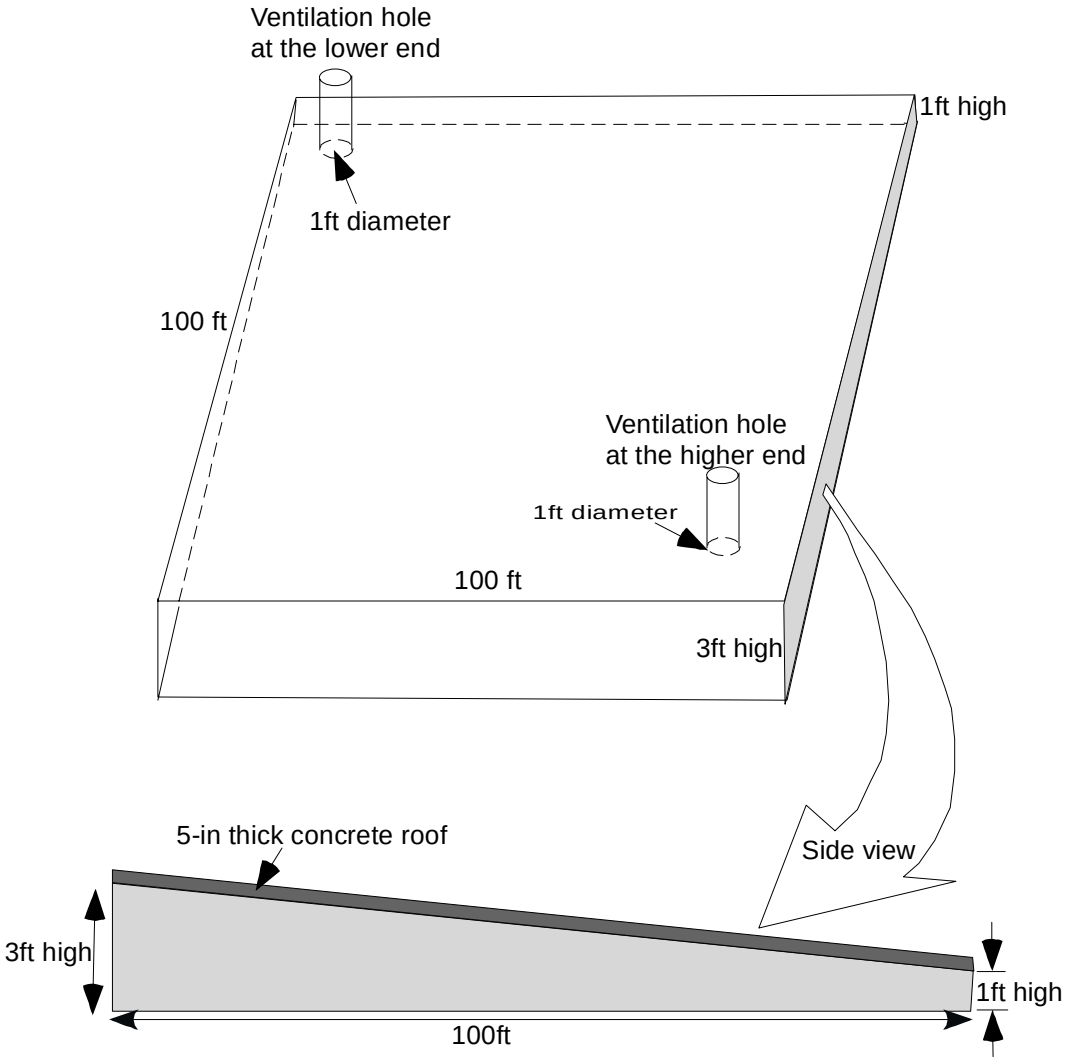

Figure 1. Modeling domain of vapor space for Saltstone Vault 4 used for the present work.

2. Modeling Approach and Analysis Method

A three-dimensional CFD approach was taken to calculate flow patterns for the gas flow patterns of Salstone Vault #4 and to examine the qualitative air circulation paths between the ambient air and vapor space gas through two breathing holes located at the roof of the vault. The detailed dimensions and geometrical information as modeled are presented in Fig. 1. A finite volume CFD code, FLUENT, was used here in creating the modeling geometry and in solving the governing equations for the present work. A computational domain of the prototypic vault geometry was non-uniformly discretized by a non-orthogonal and hexahedral mesh for the numerical simulations. Final nodes of about 150,000 meshes were established from a mesh sensitivity analysis. The modeling calculations were performed using the following assumptions:

- Typical gas flow behaviors of the vapor space in Saltstone vault due to the temperature difference between the inner roof and top grout surface are similar to the one driven by the air movement.
- Air was assumed to follow ideal gas behavior.
- Top grout surface is assumed to be flat.
- Ambient air temperature is assumed to be constant, and it is 105 F.
- The initial conditions for the vapor space are stagnant and the same as ambient temperature 105 F.

The flow conditions for the vault operations are assumed to be fully turbulent since Reynolds numbers for typical operating conditions are in the range of 24,000 based on the inlet conditions of the ventilation hole. A standard two-equation turbulence model, the κ–ε model [4], was used since previous work [5] showed that the two-equation model predicts the flow evolution of turbulent flow in a large stagnant fluid domain with reasonable accuracy. This model specifies the turbulent or “eddy” viscosity μ_t by the empirical equation.

$$\mu_t = \left(\frac{C_\mu \rho_f k^2}{\varepsilon} \right) \tag{1}$$

In eq. (1) C_μ is an empirical constant. In the present calculations, C_μ is 0.09. Thus, the turbulent viscosity is computed by solving two transport equations for k (turbulent kinetic energy) and ε (rate of dissipation of turbulent energy). The governing equations to be solved for the present work are composed of one continuity equation, three momentum equations for the three component directions (x, y, and z directions), one energy equation, and two constitutive equations for the turbulence descriptions. The detailed descriptions for the governing equations and computational methods are provided in the previous work [Ref. 3]. The model is a full three-dimensional representation of the entire gas space to capture significant phenomena related to the turbulent behavior of gas flow evolution.

Air was used to simulate the gas in the vapor space within the vault, assuming that it would give an acceptable representation of the flow patterns. Governing equations for

the entire computational domain were solved with FLUENT™ for two different cases in transient simulation mode. They are the baseline reference and the bounding cases as described in the previous section. The modeling conditions for the two cases are summarized in Table 1 and 2.

The key areas in the present analysis such as the turbulence and natural convection behaviors are benchmarked against the literature and theoretical results in order to demonstrate the adequacy of the software for the vault model since the modeling results are to support a safety significant calculation and the software is classified for more general uses.

Finally, the benchmarked modeling equations were applied to the Slatstone vault model using the computational domain as shown in Fig. 2. Design and modeling conditions are presented in Table 1 and Table 2.

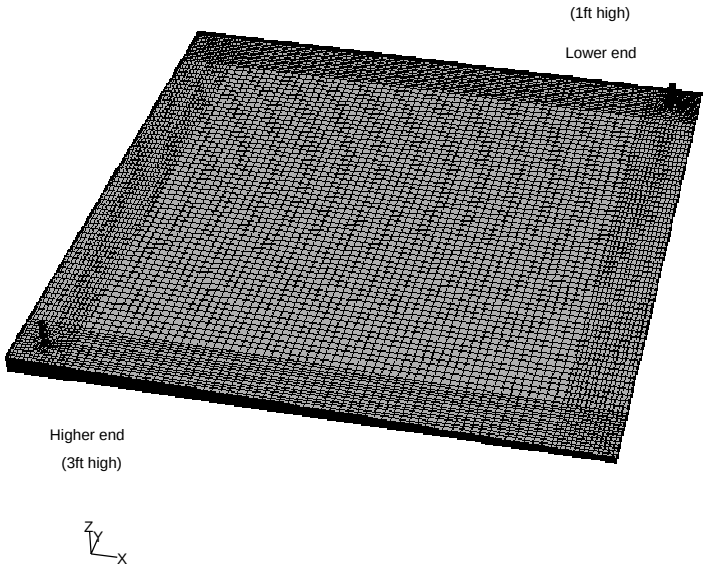

Figure 2. Three-dimensional computational domain and meshes of the vapor space of Saltstone Vault 4 as used for the present modeling calculations.

Table 1. Reference modeling conditions used for the baseline calculations in the present modeling analysis.

Parameters	Baseline reference conditions
Domain size (see Fig)	100ft x 100ft x 1 ft (lower end) X 3 ft (higher end)
Roof thickness	5 inches
Ambient temperature	105F (41C)
Initial gas temperature for vapor space	105F (41C)
Surface emissivity of roof	0.3
Solar heat flux	400 W/m2
Ventilation hole	250 Pa (2.5 mbar) gauge pressure
Ventilation hole diameter	1 ft
Chimney height of ventilation hole	4 ft
Cooling mechanism	Natural convection and radiation

Table 2. Modeling conditions for negative temperature gradient between the inner roof and top grout surface

Parameters	Input data
Domain size (see Fig. 1)	100ft x 100ft
Ambient temperature	105F (41^{o}C)
Initial temperature for gas space	105F (41^{o}C)
Inner roof surface temp	75^{o}C
Top grout surface temp	70^{o}C
Ventilation hole	250 Pa (2.5 mbar) gauge pressure*
Ventilation hole diameter	1 ft
Chimney height of ventilation hole	4 ft

Note:* Provided by WSRC-TR-2005-00071 [2]

3. Results and Discussions

The present model employed two-equation turbulence described in terms of turbulent dissipation and eddy diffusivity, and ideal gas law was used in association with natural convection mechanism for the entire computational domain as shown in Fig 2. The model is also benchmarked against the literature data and theoretical results because the modeling analysis is to support a safety significant (SS) calculation related to the flammable gas mixing inside the vapor space of Saltstone vault #4. In addition, the CFD software used in the present work is classified for more general uses.

The benchmarking tests are chosen as two typical cases representing the turbulence model and natural convection cooling behavior since these two phenomena are closely related to the gas driving mechanisms within the vapor space of Saltstone Vault #4. One is the turbulent flow calculation using the two equation model, and the other one is the natural convection calculation. The detailed descriptions of the model and results are provided in the subsequent section.

3.1 Benchmarking Results

Case 1: Turbulent isothermal flow in a pipe.

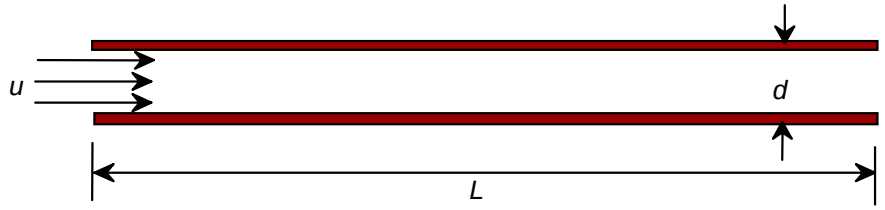

Figure 3. Isothermal flow in a circular pipe.

Figure 3 also applies to this pipe problem when water flow in a smooth pipe is assumed to be turbulent.

All of the parameters for the problem are as follows:

Water density (ρ):	1000 (kg/m^3)
Viscosity (μ):	1.71 x 10^{-3} (N.s/m^2)
Length (L):	4.0 (m)
Diameter (d):	0.2 (m)
Average speed (u):	1.710 (m/sec)

The pressure drop (ΔP) expected for this section of flow in this pipe geometry can be found from the expression,

$$\Delta P = P_{x=3m} - P_{x=4m} = \frac{1}{2}\rho u^2 \left(f \frac{L}{d} \right) \quad (2)$$

In eq. (2), $f = 0.016$ for a smooth pipe from the literature [3] for the flow condition corresponding to Re = 2.0 x 10^5. From eq. (2), the pressure drop along the distance between 3 and 4 m from the entrance is 116.96Pa for a turbulent smooth pipe.

FLUENT 6 predicted ΔP = 112.72 Pa for the circular pipe problem as shown in Table 3.

Table 3. Comparison of FLUENT 6 prediction with theoretical value.

	Theoretical Values (Pa)	FLUENT 6 Prediction (Pa)	Relative Error (%)
Prob. 1-C	116.96	112.72	3.63

Case 2: Two-dimensional natural convection inside a rectangular enclosure with specified boundary temperatures

The two-dimensional natural convection problem with specified boundary temperatures consists of a rectangular enclosure with adiabatic horizontal walls and isothermal vertical walls maintained at a fixed temperature difference. The temperature differences between the hot and cold walls are 10K for the first case and 25K for the second case. The model calculation is based on conduction and natural convection of heat through the gas medium. The height and width of the enclosure were arbitrarily chosen to be 0.5m and 0.0254m, respectively, which is corresponding to the aspect ratio of about 20 considered as a narrow slit geometry. A schematic of this problem is shown in Fig. 4.

An analytical solution for the natural convection problem can be determined for an idealized representation of the problem as fully developed flow between two infinite parallel plates as shown in Fig. 4. The momentum and energy equations for this two-dimensional problem can be expressed in the following form:

$$g\beta(T - T_m) + \left(\frac{\mu}{\rho}\right)\left(\frac{\partial^2 u}{\partial x^2}\right) = 0 \quad (3)$$

$$\left(\frac{\partial^2 T}{\partial x^2}\right) = 0 \quad (4)$$

where u is the y-direction component of the velocity and the Boussinesq approximation has been applied to the gravitational term of eq. (4). The reference temperature for the problem is taken as

$$T_m = \frac{1}{2}(T_H - T_L) \quad (5)$$

With the boundary conditions

$T = T_H$ at x = 0 and $T = T_L$ at x = L,

the energy equation can be solved to give

$$T(x) = T_H - (T_H - T_L)\left(\frac{x}{L}\right) \quad (6)$$

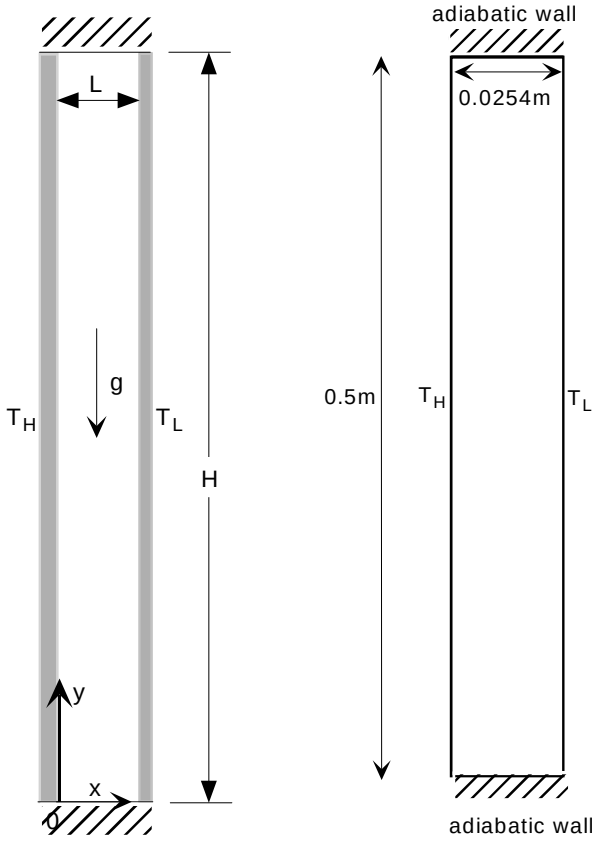

Figure 4. Natural convection test section inside a slit enclosure.

Substituing eq. (5) and (6) into eq. (3) results in

$$\frac{d^2u(x)}{dx^2}=\left(\frac{g\beta\rho}{\mu}\right)(T_H-T_m)\left(2\frac{x}{L}-1\right) \tag{7}$$

Integrating once gives

$$\frac{du(x)}{dx}=\left(\frac{g\beta\rho}{\mu}\right)(T_H-T_m)\left(\frac{x^2}{L}-x\right)+A \tag{8}$$

Integrating a second time gives

$$u(x)=\left(\frac{g\beta\rho}{\mu}\right)(T_H-T_m)\left(\frac{x^3}{3L}-\frac{x^2}{2}\right)+Ax+B \tag{9}$$

Using no-slip boundary condition (u(x) = 0) at x = 0 and x = L allows the constants A and B of eqs. (8) and (9) to be determined.

$$A = \frac{g\beta\rho}{6\mu} L(T_H - T_m)$$

$$B = 0 \qquad (10)$$

Substituting the constants of eq. (10) into eq. (9) results in the following expression for u(x):

$$u(x) = \left(\frac{g\beta\rho}{12\mu}\right) L^2 (T_H - T_L) \left\{ 2\left(\frac{x}{L}\right)^3 - 3\left(\frac{x}{L}\right)^2 + \left(\frac{x}{L}\right) \right\} \qquad (11)$$

This expression shows extrema at x/L = 0.211 and 0.789. The magnitude of the term in brackets at the extrema is ± 0.0962. This value can be multiplied by the physical constants in eq. (11) and compared to numerical results. The physical constants are

$\rho = 0.1626\ kg/m^3$

$\beta = 2.85x10^{-3}\ K^{-1}$

$g = 9.81\ m/\sec^2$

$\mu = 2.0x10^{-5}\ N - \sec/m^2$

$L = 0.0254\ m$

With these values, the maximum velocity at the mid-plane of the rectangular enclosure is theoretically

Case A: u = $\pm$ 0.01176 m/sec for $\Delta T = (T_H - T_L) = 10K$

Case B: u = $\pm$ 0.02939 m/sec for $\Delta T = (T_H - T_L) = 25K$

The profile of velocity across the width of the gap is as important as the maximum value within the gap of the slit geometry. Figure 5 and Figure 6 show the profile comparison for these two cases. Table 4 also shows comparison of the peak values predicted by FLUENT 6 with the theoretical ones.

Table 4. Comparison of maximum velocities predicted by FLUENT 6 and theoretical values.

Cases	Theoretical Values (m/sec)	FLUENT 6 Prediction (m/sec)	Relative Error (%)
Case A	0.01176	0.01129	2.84
Case B	0.02939	0.02822	2.96

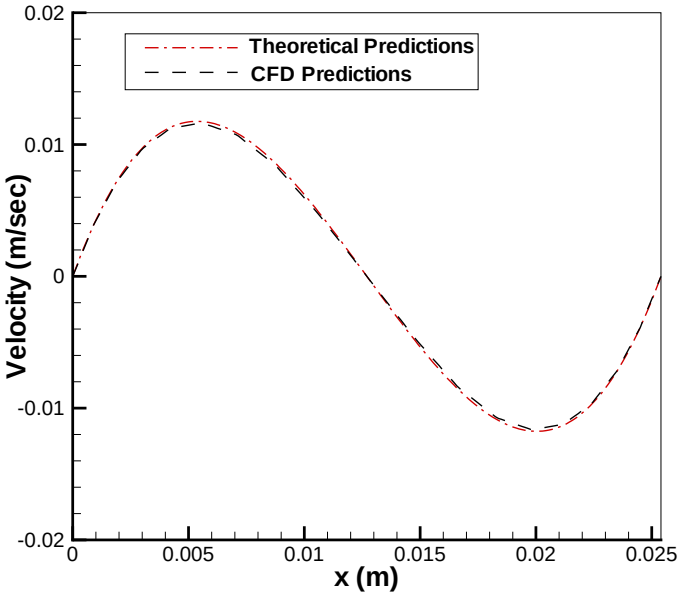

Figure 5. Comparison of FLUENT6 predictions with theoretical predictions for Case A

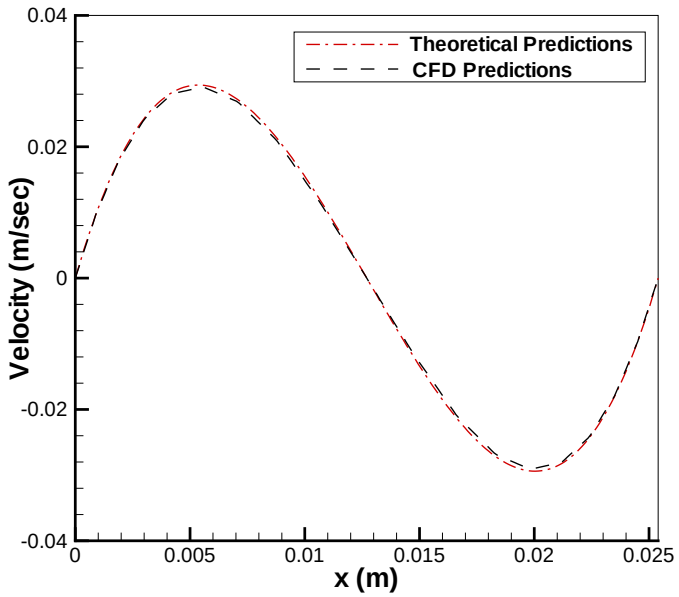

Figure 6. Comparison of FLUENT6 predictions with theoretical predictions for Case B

3.2 Results for the Saltstone Vault Model

The turbulence behavior and natural convection mechanism used in the present model were benchmarked against the literature information and theoretical results in the previous section. The verified model was applied to the Saltstone vault geometry for the transient assessment of the gas flow patterns inside the vapor space of the vault region using the boundary conditions as provided in Tables 1 and 2.

The present model considered two cases for the estimations of the flow patterns within the vapor space. One is the baseline reference case provided in Table 1. The other is for the negative temperature gradient between the roof inner and top grout surface temperatures intended for the potential bounding condition, which is provided in Table 2. Pressures at both holes are assumed to be maintained as 250 Pa gauge pressure given by the literature data [2]. As the initial conditions for the present transient simulations, the vapor space is assumed to be stagnant at ambient temperature 105 F.

At 7 hours transient time since the beginning of the initial conditions, the temperature contours for the plane crossing the lower inlet hole is shown in Fig. 7. It is clearly shown that the ambient cooler air comes into the vapor space domain through the ventilation hole of the lower end, and then it hits the top surface of the grout region. Figure 8 presents the temperature distributions for the plane crossing the ventilation holes near the corner of the higher end. The transient results show that maximum temperature of the roof inner wall is still about 10^{o}C lower than the top grout surface temperature, which is provided as 70^{o}C boundary condition shown in Table 1. This case corresponds to positive temperature gradient between the roof inner and top grout surface temperatures. In this case, the velocity flow patterns corresponding to the temperature distributions are shown in Figs. 9 and 10. The flow pattern results confirmed the air circulations through the two holes. It is noted that the ambient air of about 41^{o}C (105 F) comes into the gas space through the lower end hole, and after it is heated up to 64^{o}C (147 F) at 7 hours transient time, it comes out of the vault via the higher end one.

Density distributions along the diagonal plane crossing the two ventilation holes are shown in Fig. 11. Figure 12 confirms that heavier air comes into the hole located near the corner of the lower end region. Temperature distributions at the entire plane crossing the middle elevation of the vapor space are shown in Fig. 13. As shown in Fig. 14, density distribution patterns are very similar to the temperature distributions, showing the local cell patterns. These results are consistent with the literature information. Velocity flow patterns at the mid-plane of the vapor space inside the vault are also shown in Fig. 15. It is noted that the flow patterns consists of small cells like honey comb as the ambient cooler air gets heated up during the residence time inside the vault. Maximum speed of air movement is at the two ventilation holes of the vault, and it reaches about 1.2 m/sec (~4 ft/sec). Detailed results are shown in Fig. 16.

As the second case, the potential negative temperature gradient is considered as the bounding case. This case corresponds to the case that the inner roof surface temperature is higher than the top grout surface temperature. The conditions for the negative temperature gradient model are given in Table 2. Figure 17 and Figure 18 show temperature distributions near the two ventilation holes at the higher and lower ends of the vault after the 90-second transient period of the negative temperature gradient. The results show that the vapor space near the lower end region gets heated more quickly than the higher end region since the heat transfer mechanism at early transient period is controlled primarily by the conduction mode. As shown in Figs. 19

and 20, the gas contained inside the vapor space of the vault is breathing out through both of the two holes because of the dominant gas buoyancy. Figure 21 shows vertical velocity distributions along the vertical distance from the top grout surface to the roof of the vault. Positive velocity In the figure indicates the gas flow leaving the vapor space through the ventilation hole.

When the transient time reaches about 3 minutes, the ambient air starts to flow into the vapor space of the vault via the lower-end hole and to flow out through the higher-end hole. As shown in Figs. 22 and 23, the air circulation patterns are formed through both ventilation holes. Figure 24 shows that flow patterns for this case are very similar to those of the first case, the positive temperature gradient. Temperature contour plots confirm the consistent circulation patterns in terms of gas energy exchanges for both breathing holes as presented in Figs. 25 and 26.

The conclusive flow patterns of the vapor space obtained by the CFD modeling results are summarized in Fig. 27 in a qualitative way, which is consistent with the literature information [6]. Table 5 summarizes the quantitative results for the air flowrates coming into the vapor space through the ventilation hole near the lower end of the vault under the two modeling conditions considered in the present work

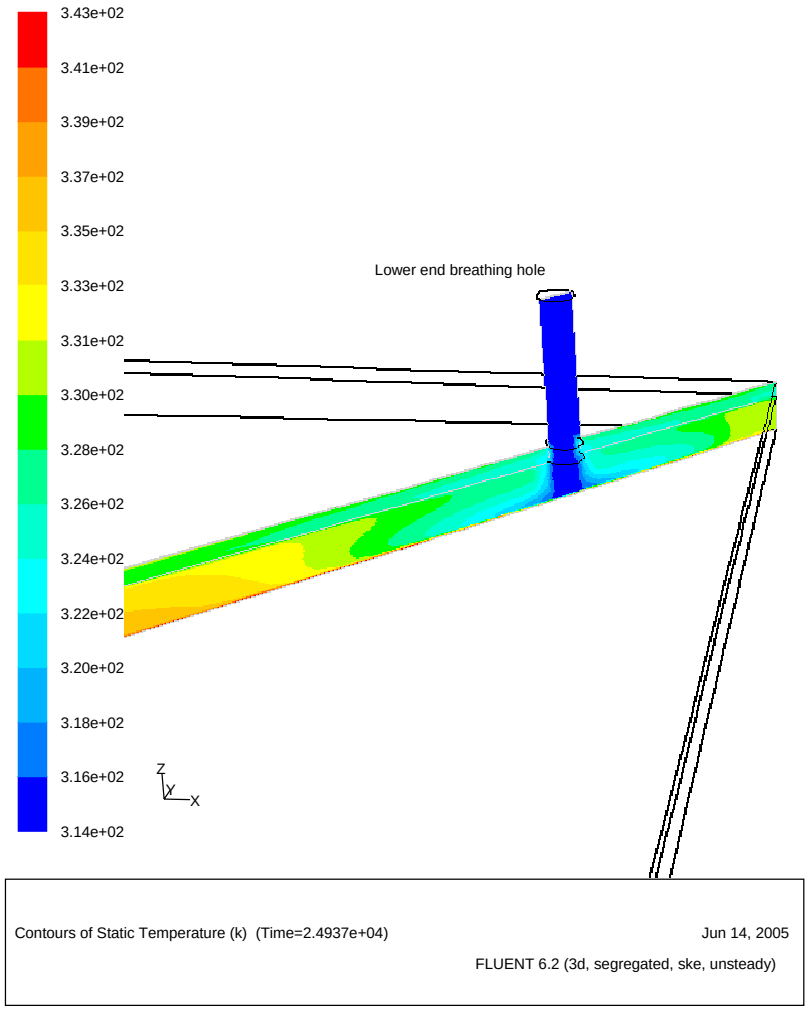

Figure 7. Temperature contours near the lower end breathing hole at t = 7 hours

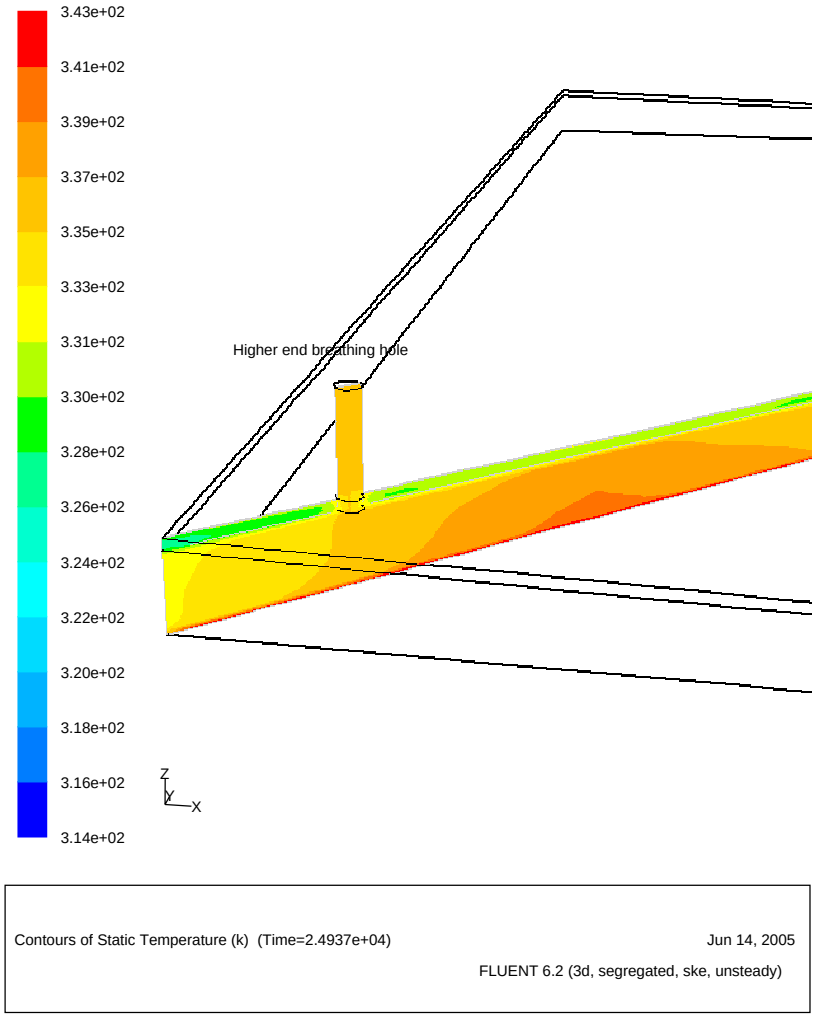

Figure 8. Temperature contours near the higher end breathing hole at t = 7 hours

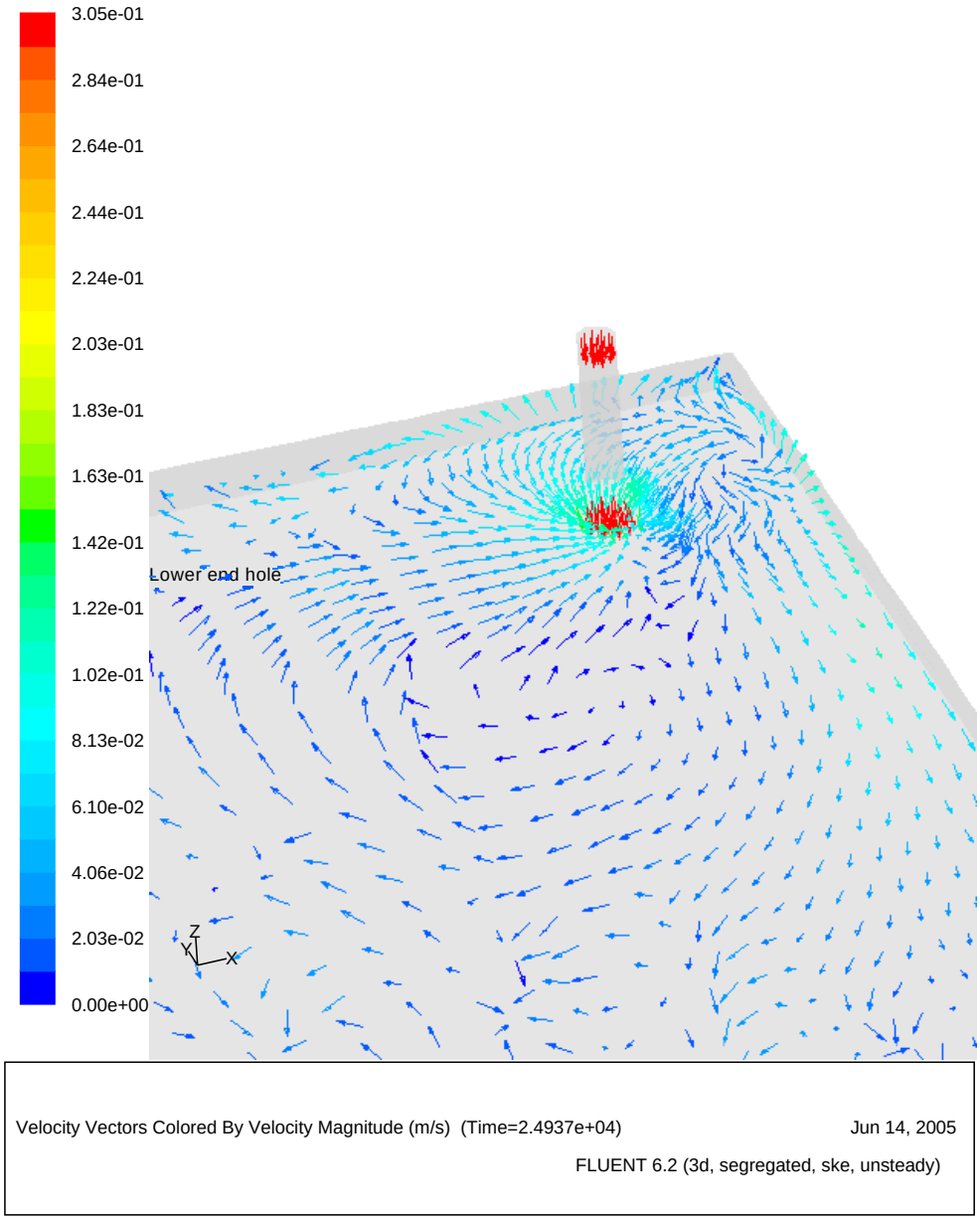

Figure 9. Flow patterns near the lower end breathing hole at t = 7 hours

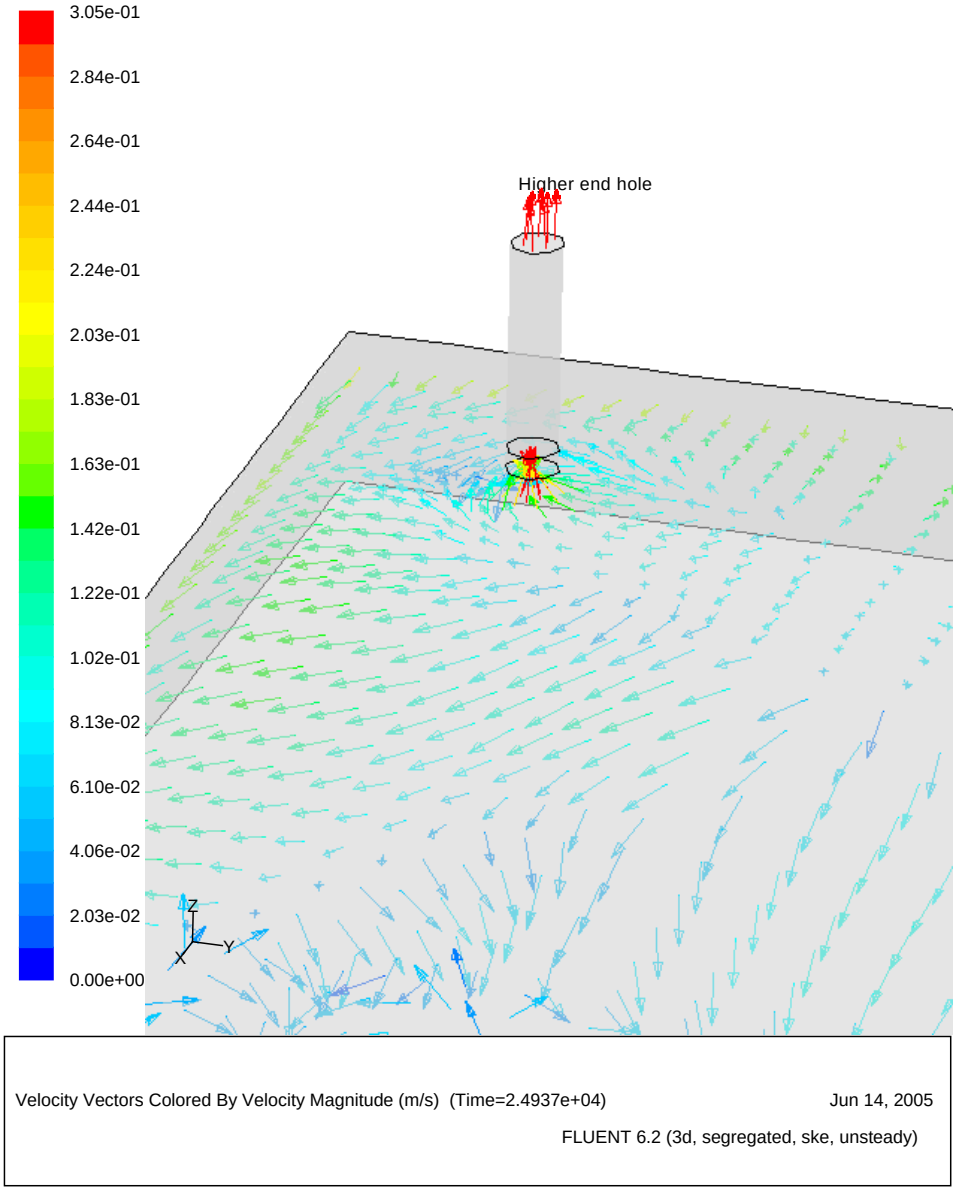

Figure 10. Flow patterns near the higher end breathing hole at t = 7 hours

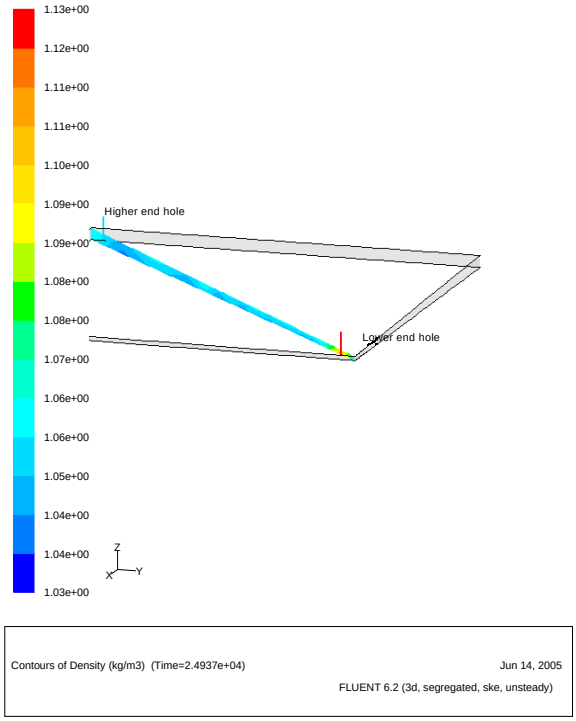

Figure 11. Density distributions along the diagonal plane crossing the two ventilation holes

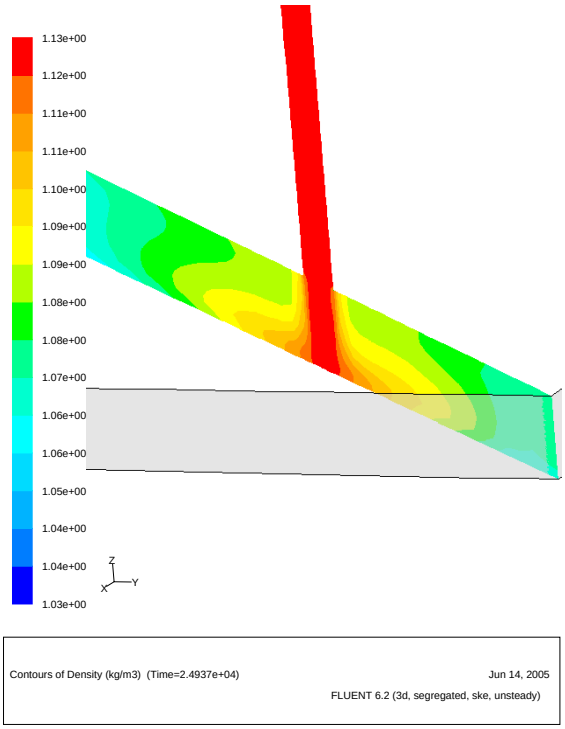

Figure 12. Density distributions near the lower end breathing hole at t = 7 hours showing the ambient heavier air is drawing into the vapor space of the Saltstone vault

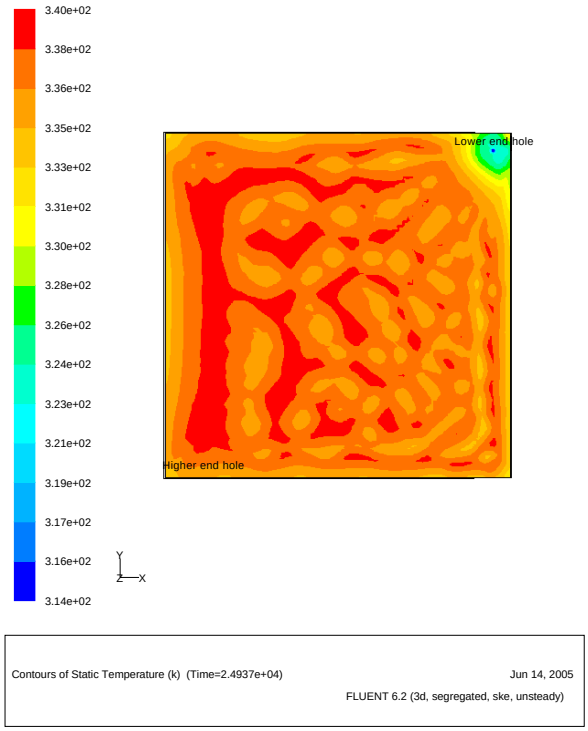

Figure 13. Temperature distributions at the mid-plane of the gas space showing the honeycomb-type heat transfer

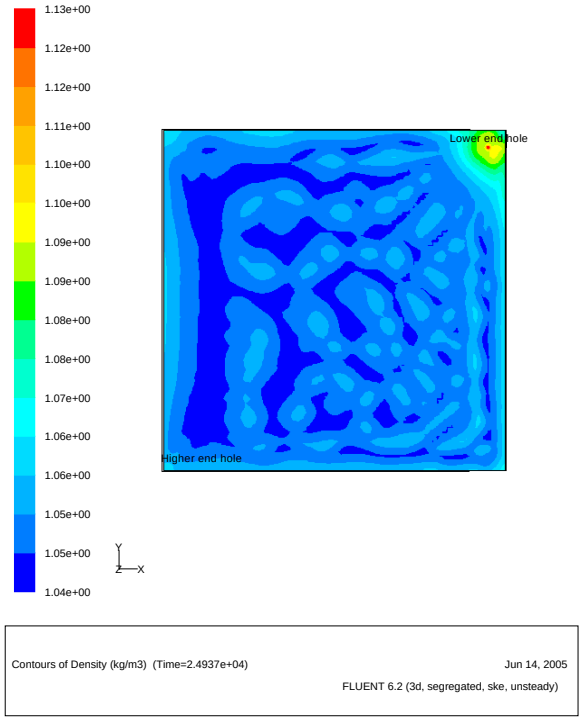

Figure 14. Density distributions at the mid-plane of the gas space showing the honeycomb-type heat transfer

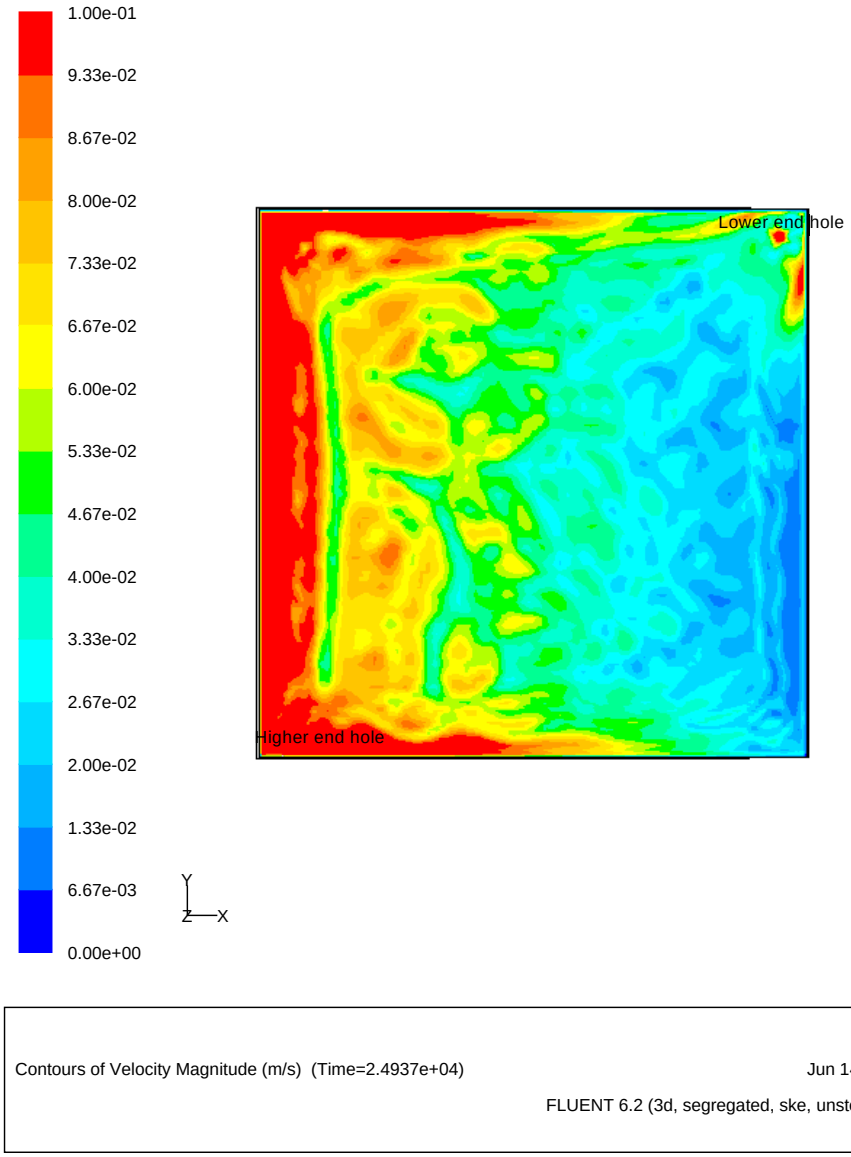

Figure 15. Velocity flow patterns at the mid-plane of the vapor space inside the vault

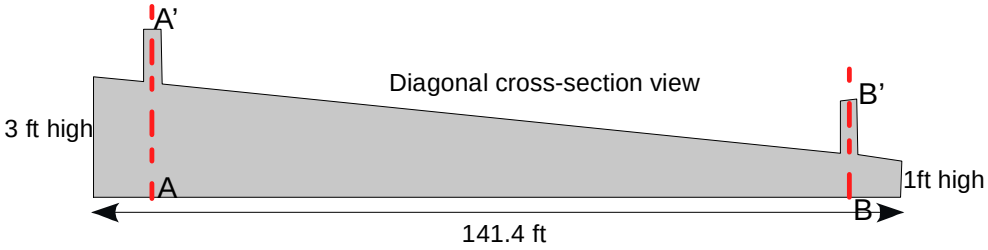

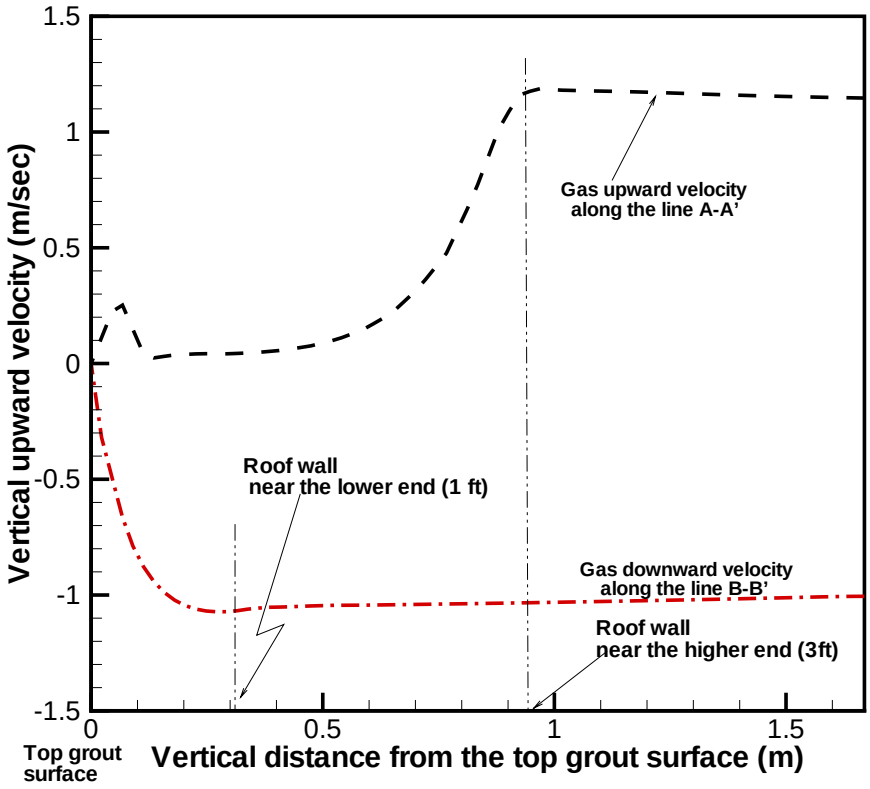

Figure 16. Gas upward velocity profile along the vertical lines A-A' and B-B' of the two ventilation holes indicating that the lower end hole has downward airflow patterns

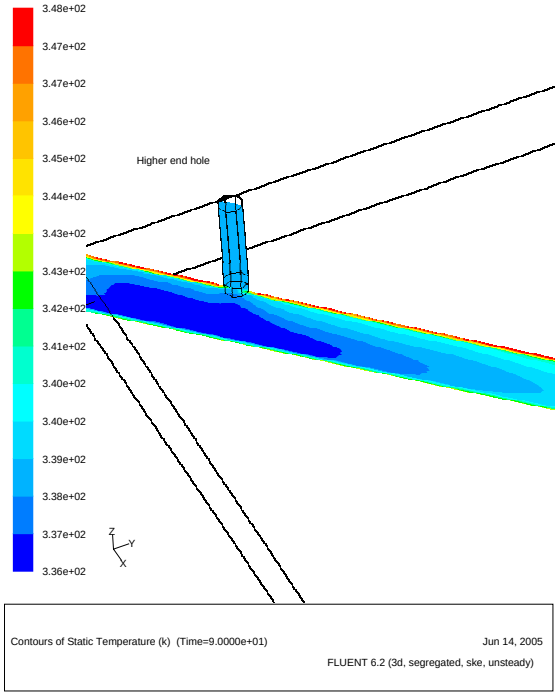

Figure 17. Temperature distributions near the ventilation hole at the higher end of the vault during the 90 second transient period of the negative temperature gradient

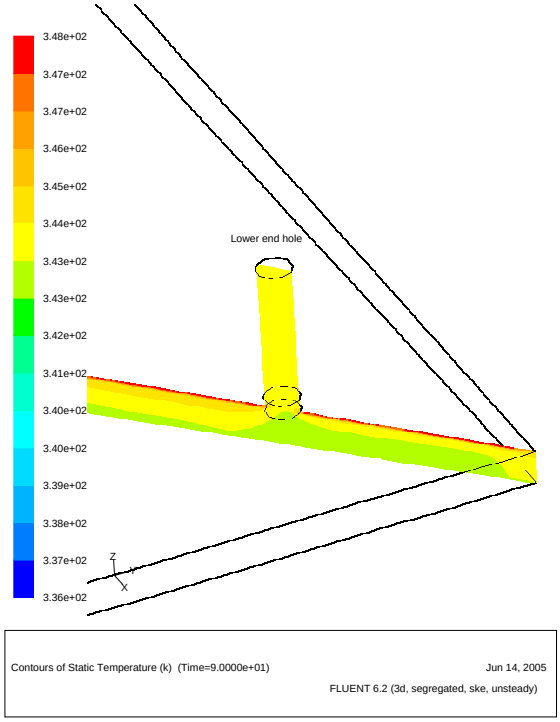

Figure 18. Temperature distributions near the ventilation hole at the lower end of the vault during the 90 second transient period of the negative temperature gradient

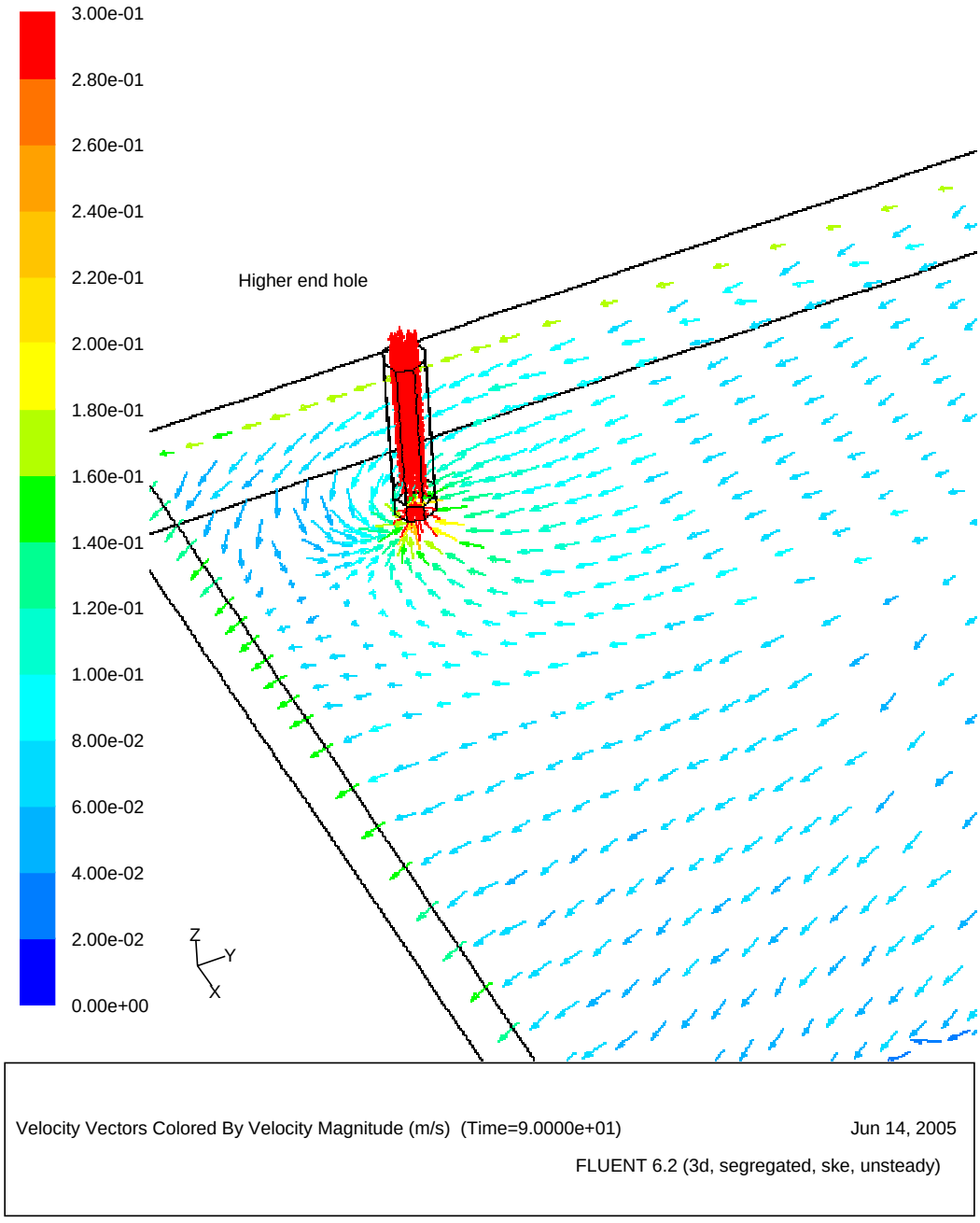

Figure 19. Flow patterns near the ventilation hole at the higher end of the vault during the 90 second transient period of the negative temperature gradient

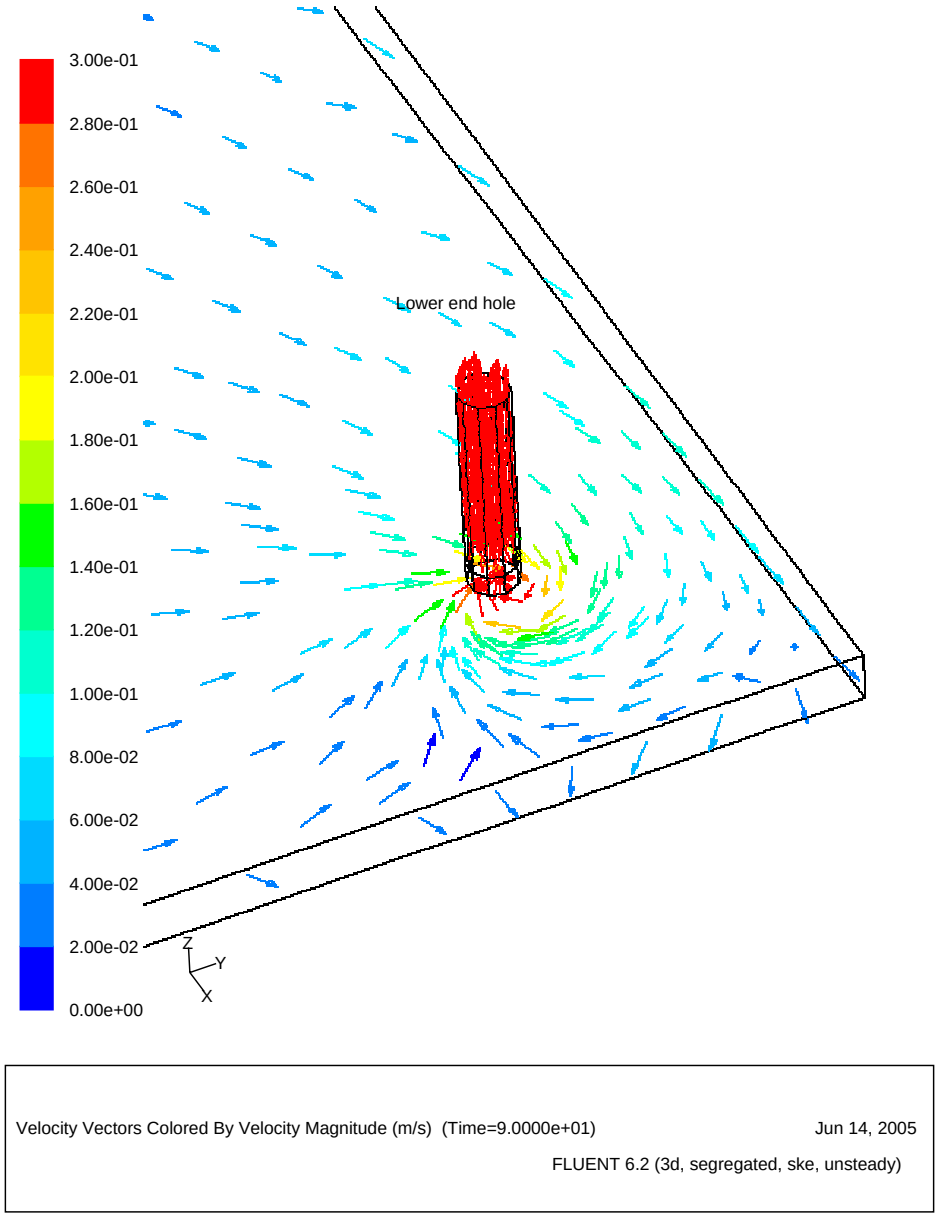

Figure 20. Flow patterns near the ventilation hole at the lower end of the vault during the 90 second transient period of the negative temperature gradient

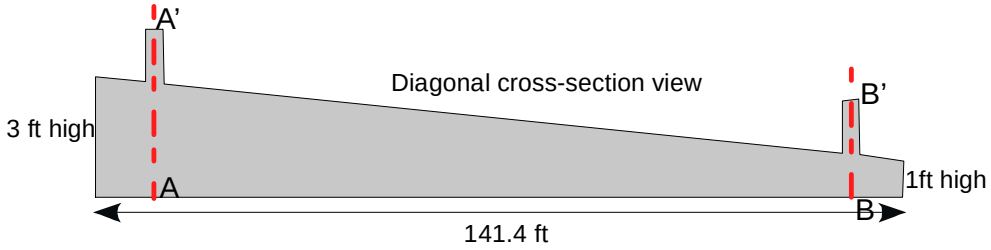

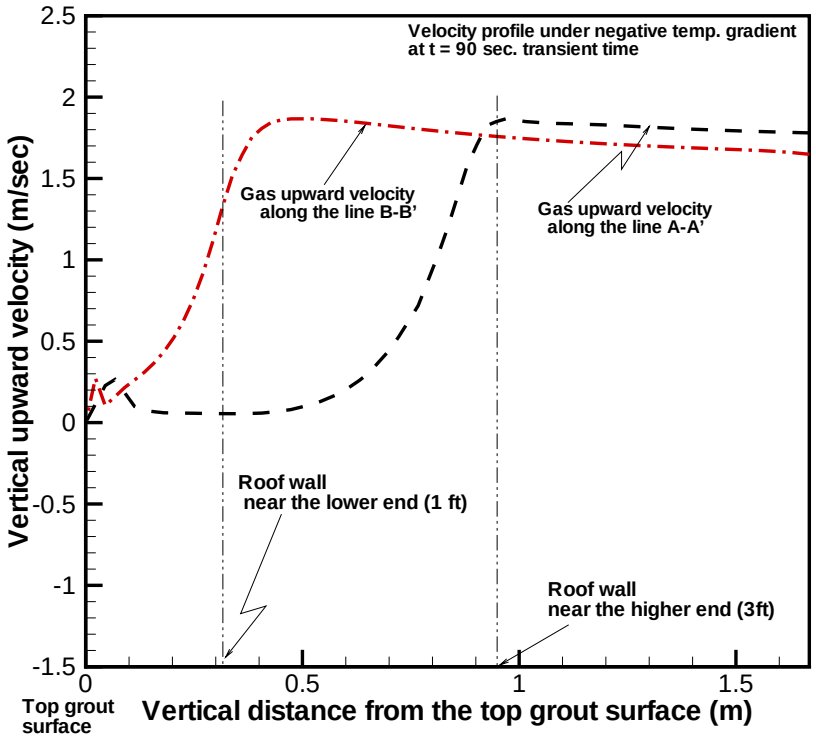

Figure 21. Gas upward velocity profile along the vertical lines A-A' and B-B' of the two ventilation holes under the negative temperature gradient between the inner roof and top grout surface during early transient period (90 seconds of transient time), indicating that both of the lower and higher holes have upward airflow patterns

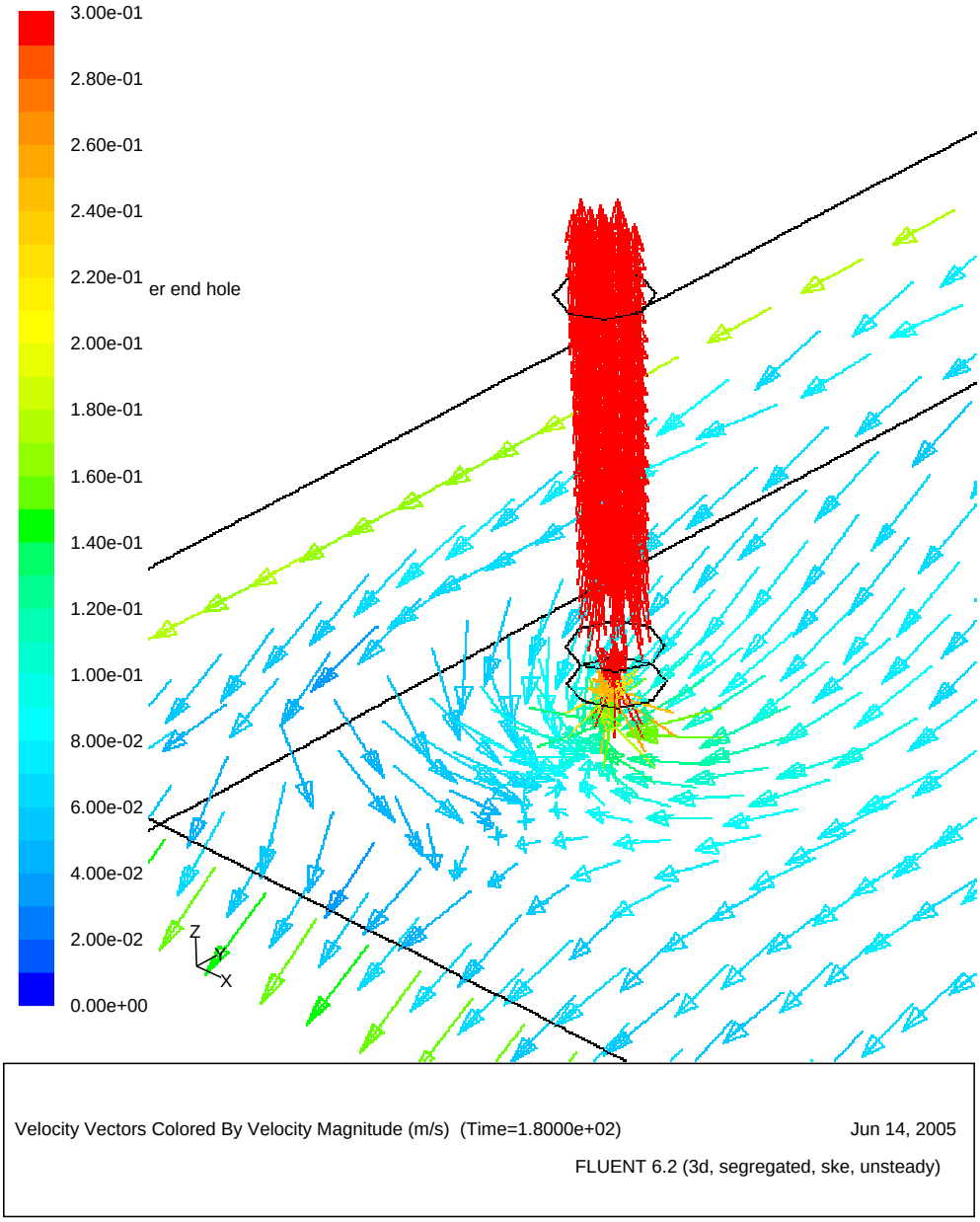

Figure 22. Flow patterns near the ventilation hole at the higher end of the vault during the 180 second transient period of the negative temperature gradient

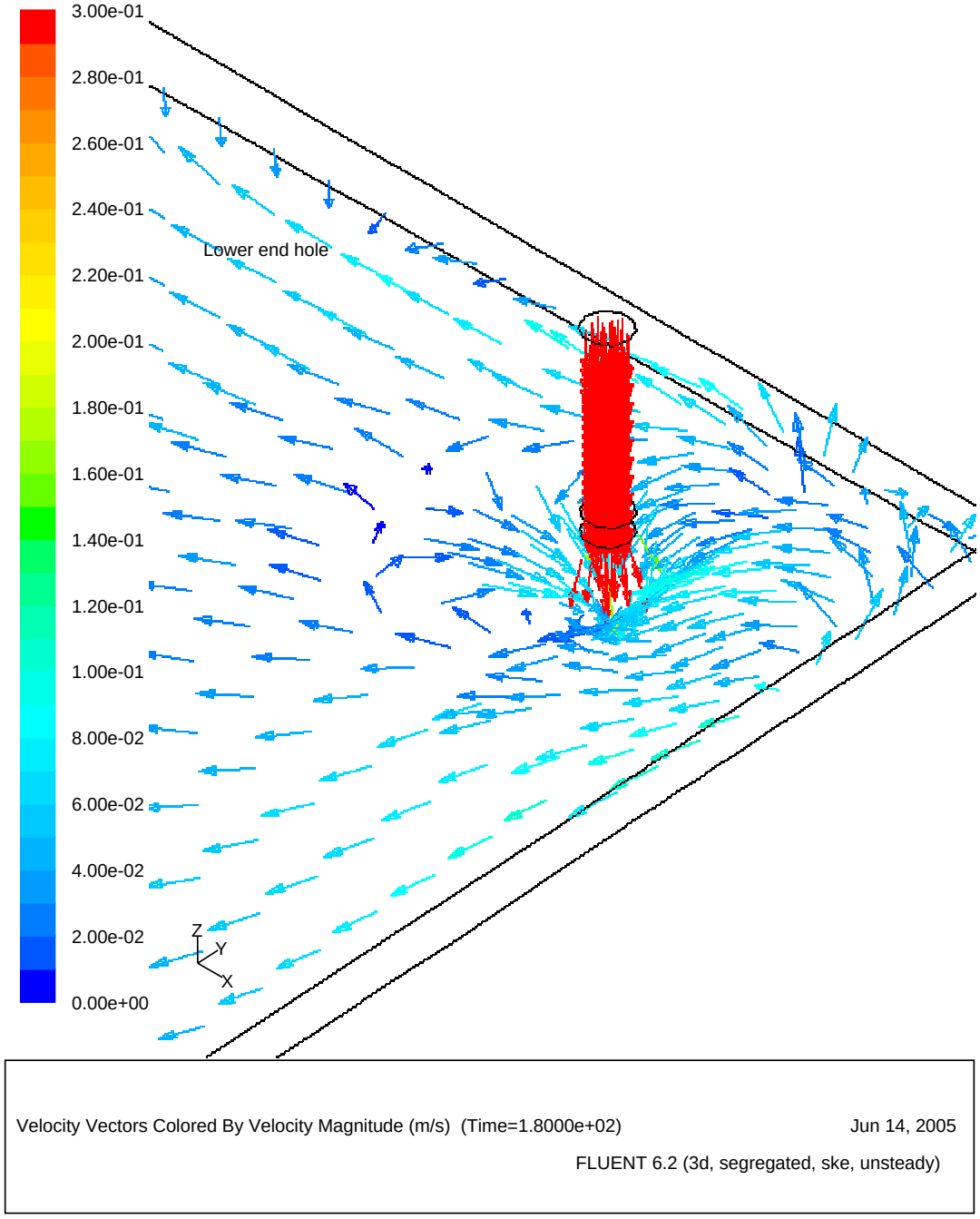

Figure 23. Flow patterns near the ventilation hole at the lower end of the vault during the 180 second transient period of the negative temperature gradient

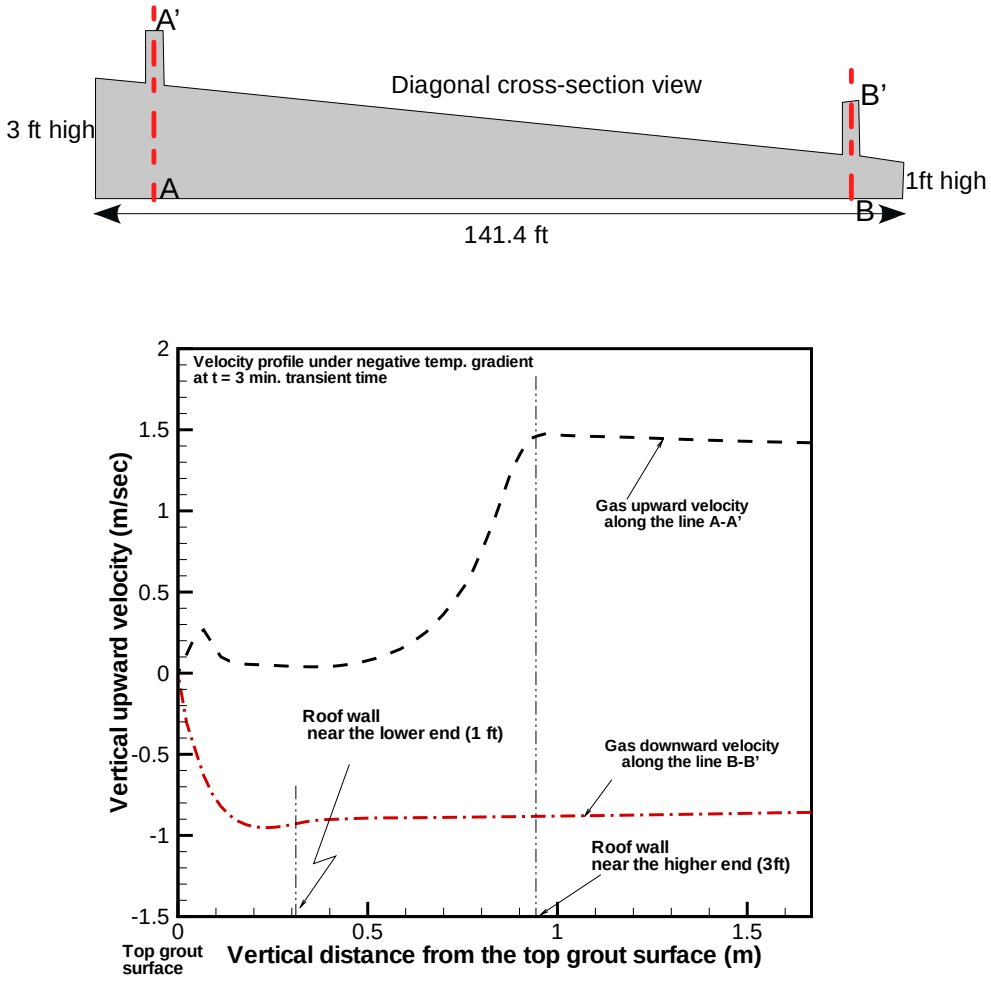

Figure 24. Gas upward velocity profile along the vertical lines A-A' and B-B' of the two ventilation holes under the negative temperature gradient between the inner roof and top grout surface at 3-minute transient time, noting that the lower end hole has the gas flow patterns switched from the upward flow of the 90-second transient to the downward one of the later transient

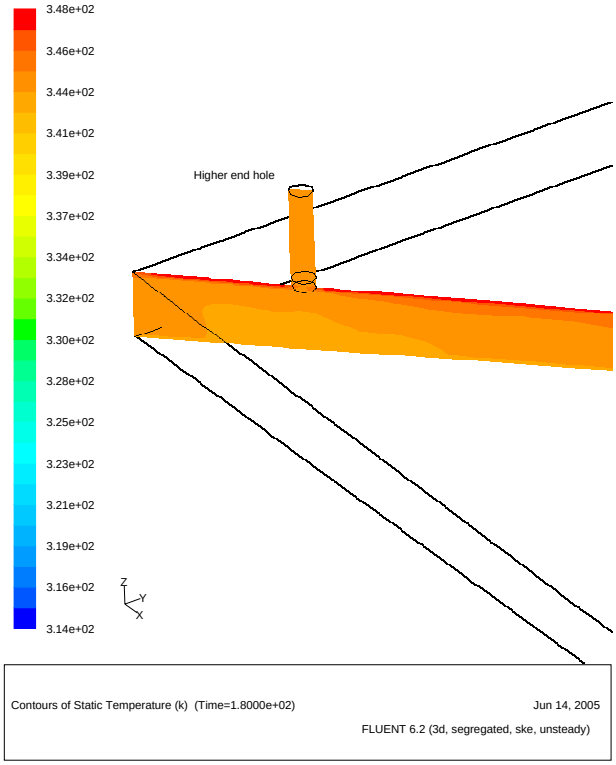

Figure 25. Temperature contours near the ventilation hole at the lower end of the vault during the 180 second transient period of the negative temperature gradient showing that the hot gas is leaving the vapor space through the ventilation hole

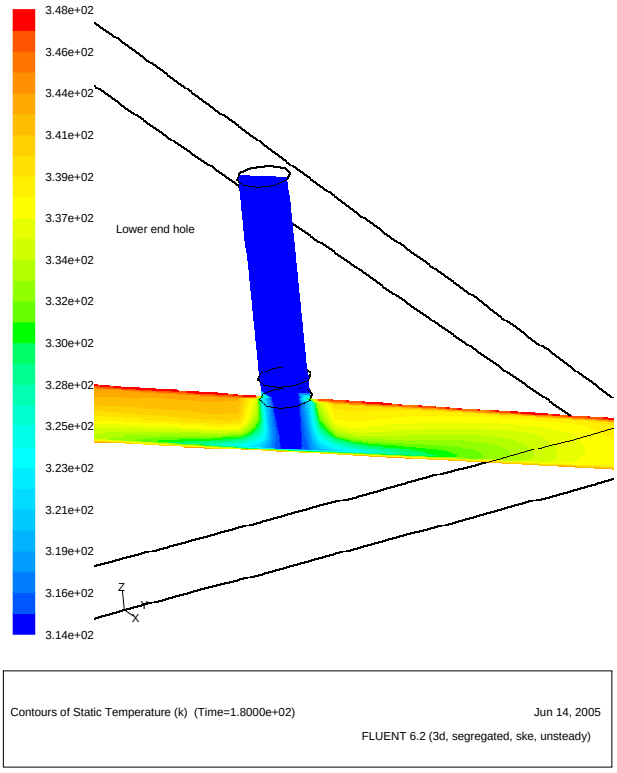

Figure 26. Temperature contours near the ventilation hole at the lower end of the vault during the 180 second transient period of the negative temperature gradient showing that the vapor space region near the ventilation hole of the lower end has ambient temperature

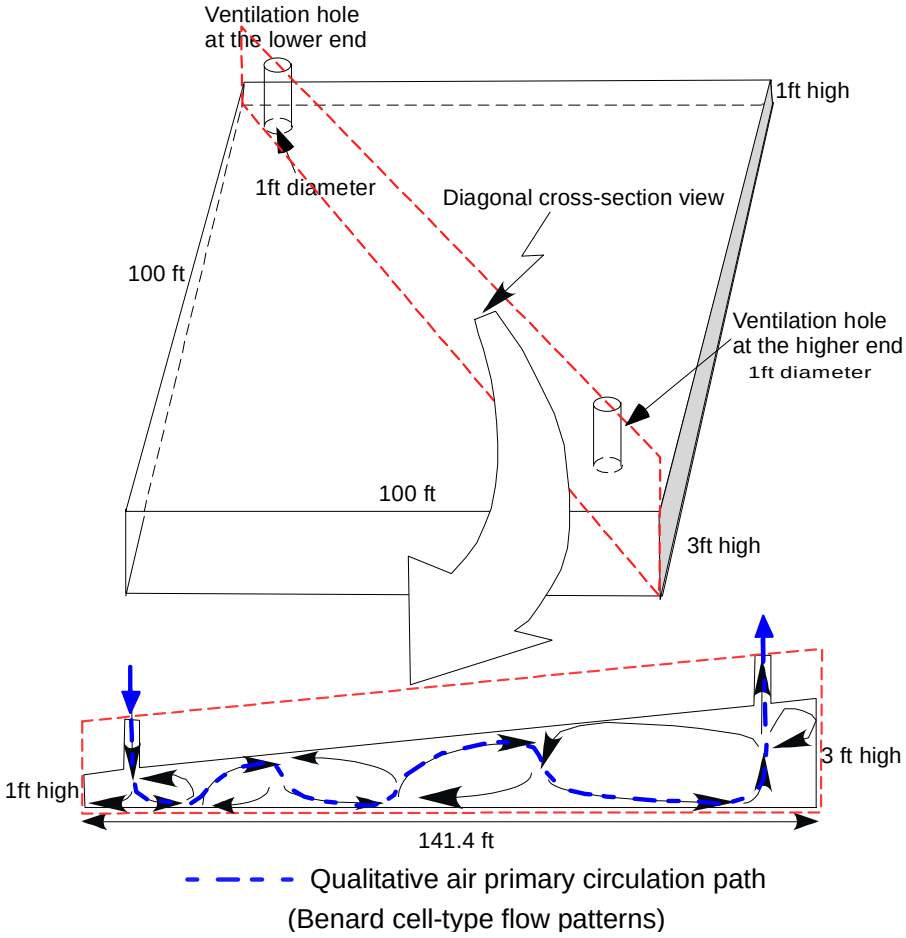

Figure 27. Qualitative gas circulation patterns obtained by the present CFD modeling calculations for the vapor space of Saltstone vault #4, showing that the ambient air comes into the vapor space of the vault through the ventilation hole located near the lower end

Table 5. Quantitative results for the air flowrate coming into the vapor space through the ventilation hole near the lower end of the vault under the two modeling conditions considered in the present work

Cases	Modeling transient time	Average air velocity coming into the vapor space within the vault	Air flowrate coming into the vapor space via the lower inlet hole (1-ft diameter)
Positive temperature gradient*	7 hours	2.16 (ft/sec)+	760 gpm
Negative temperature gradient**	3 minutes	1.84 (ft/sec)+	648 gpm

Note:* Reference modeling conditions as provided by Table 1

** Modeling conditions for the negative temperature gradient as provided by Table 2

+ Average flow velocity (V_{avg}) was computed by averaging local velocity v over the ventilation hole area (A_{hole}):

$$V_{avg} = \frac{1}{A_{hole}} \int_{A_{hole}} v \, dA$$

4. Conclusions

A computational fluid dynamics (CFD) method was applied to estimate the flow patterns for vapor space domain inside the Saltstone Vault #4. The CFD model took a three-dimensional transient momentum-energy coupled approach. The flow conditions for the vault operations are assumed to be fully turbulent since Reynolds numbers for typical operating conditions are in the range of 24,000 based on the inlet conditions of the ventilation hole. A standard two-equation turbulence model was used for this work.

The turbulence behavior and natural convection mechanism used in the present model were benchmarked against the literature information and theoretical results for the present work. The verified model was applied to the Saltstone vault geometry for the transient assessment of the gas flow patterns inside the vapor space of the vault region using the boundary conditions as provided by the customer.

The present model considered two cases for the estimations of the flow patterns within the vapor space. One is the reference baseline case. The other is for the negative temperature gradient between the roof inner and top grout surface temperatures intended for the potential bounding condition. The flow patterns of the vapor space calculated by the CFD model demonstrate that the ambient air comes into the vapor space of the vault through the lower-end ventilation hole, and it gets heated up by the Benard-cell type circulation before leaving the vault via the higher-end hole. The calculated results are consistent with the literature information.

5. References

1. A. V. Staub, TTR, HLW-SSF-TTR-2005-0008, June 23, 2005.

2. A. S. Choi, “An Order-of-Magnitude Estimation of Benzene Concentration in Saltstone Vault”, WSRC-TR-2005-00071 Rev. 0, February 2005.

3. Bird, R. B., Stewart W. E., and Lightfoot, E. N., *Transport Phenomena*, John Wiley & Sons, New York, 1960.

4. *FLUENT6*, Fluent, Inc., 2005.

5. S. Y. Lee, R. A. Dimenna, D. B. Stefanko, R. A. Leishear, “Mixing in Large Scale Tanks – Part I, Flow Modeling of turbulent Mixing Jets,” ASME Heat Transfer / Fluids Engineering Conference, Charlottee, N. C., July 11 – 15, 2004.

6. J. P. Holman, *Introduction to Heat Transfer*, Hemisphere Publishing Co., New York, 1969.